Supporting Information

Construction of Three-Dimensional $CuCo_2S_4$/CNT/graphene Nanocomposite for High Performance Supercapacitors

Jianfeng Shen[1,2], Jianhua Tang[1], Pei Dong[2], ZhuQing Zhang[1], Jin Ji[1], Robert Baines [2], Mingxin Ye[1,*]

[1] Institute of special materials and technology, Fudan University, 200433, Shanghai, China

[2] Department of Materials Science and NanoEngineering, Rice University, 6100 Main Street, Houston, TX 77005, USA

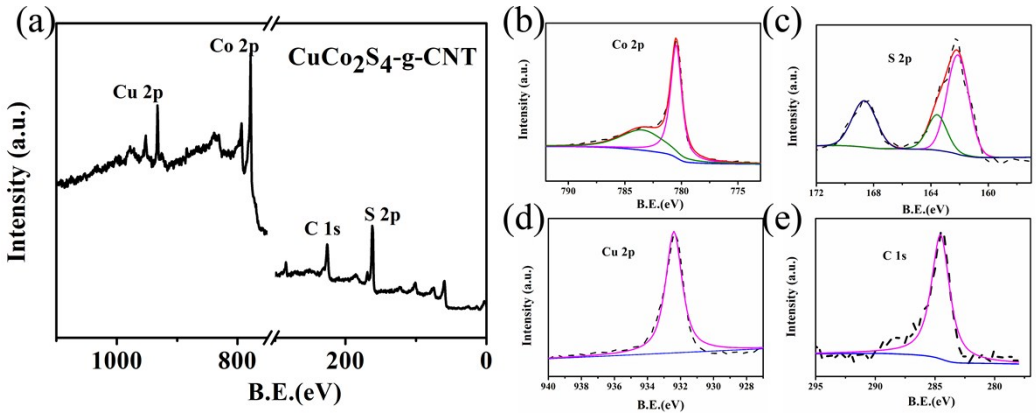

Figure S1 XPS survey spectrum of $CuCo_2S_4$-g-CNT (a). High-resolution XPS spectra of Co 2p (b), S 2p (c), Cu 2p (d), and C 1s (e) of $CuCo_2S_4$-g-CNT.

To further assess the near-surface elemental composition and the chemical state of the as-prepared $CuCo_2S_4$-g-CNT 3D structure, X-ray photoelectron spectroscopy (XPS) measurements were conducted. The results are presented in Figure S1. Employing Gaussian fitting method, the Co 2p spectrum can be fitted with two spin orbit doublets, characteristic of Co^{2+} and Co^{3}. The S 2p spectrum can be divided into one shakeup satellite and two main peaks, while the Cu $2p_{3/2}$ spectrum is found at 932.5 eV. As to C1s spectrum, it is found at 284.5 eV, relating to the C=C on graphene and CNTs.

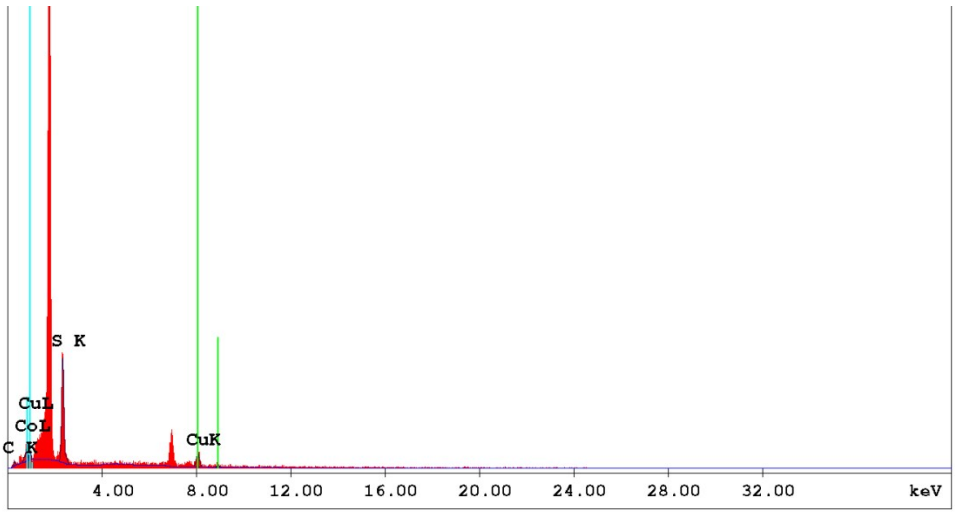

Figure S2 EDX pattern of $CuCo_2S_4$-g-CNT.

Table S1 Elements ratio of $CuCo_2S_4$-g-CNT

Element	Wt %	At %
C K	33.34	65.11
Co L	27.77	11.05
S K	26.19	19.15
Cu K	12.70	4.69
Total	100.00	100.00

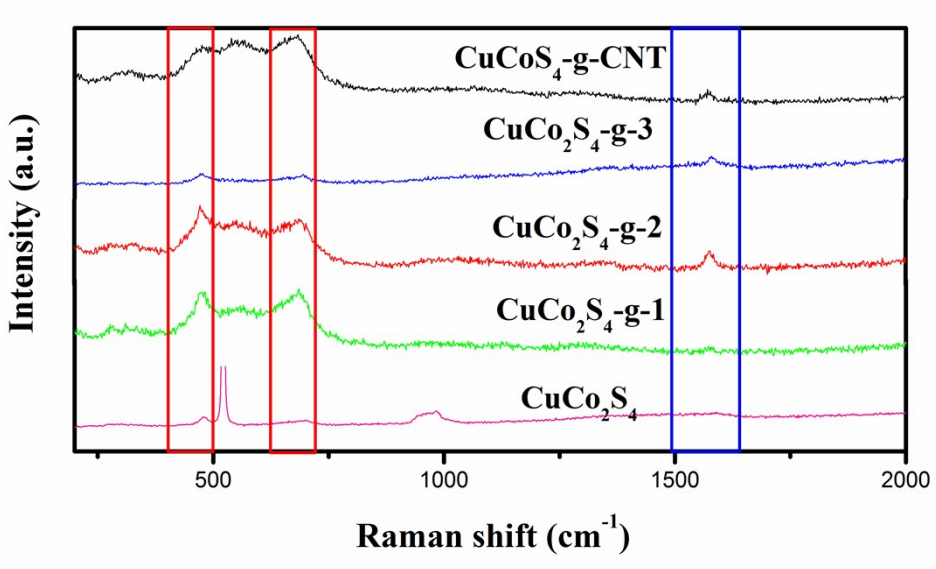

Figure S3 Raman spectra of $CuCo_2S_4$, $CuCo_2S_4$-g and $CuCo_2S_4$-g-CNT.

Figure S3 demonstrates Raman spectra of $CuCo_2S_4$, $CuCo_2S_4$-g and $CuCo_2S_4$-g-CNT. The peaks between 300-1000 cm^{-1} (red) are attributed to $CuCo_2S_4$, while the peak around 1620 cm^{-1} (blue) can be assigned to graphene and CNTs.

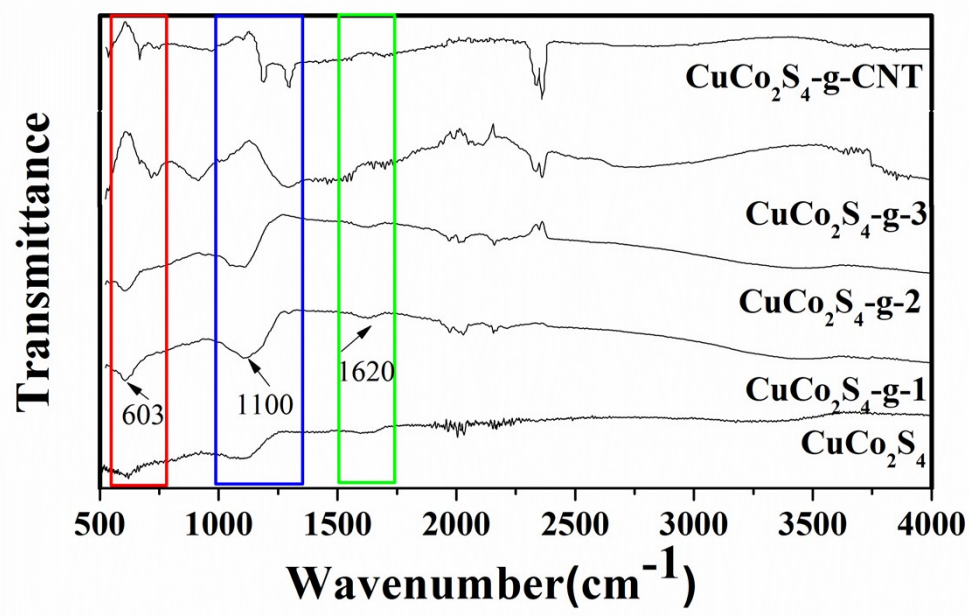

Figure S4 FTIR spectra of $CuCo_2S_4$, $CuCo_2S_4$-g and $CuCo_2S_4$-g-CNT

Figure S4 demonstrates the FTIR spectra of $CuCo_2S_4$, $CuCo_2S_4$-g and $CuCo_2S_4$-g-CNT. The peaks between 500-1200 cm^{-1} (red and blue) are attributed to the vibration of Cu-S and Co-S, while the peak around 1620 cm^{-1} (green) can be assigned to C-C vibration of graphene and CNTs.

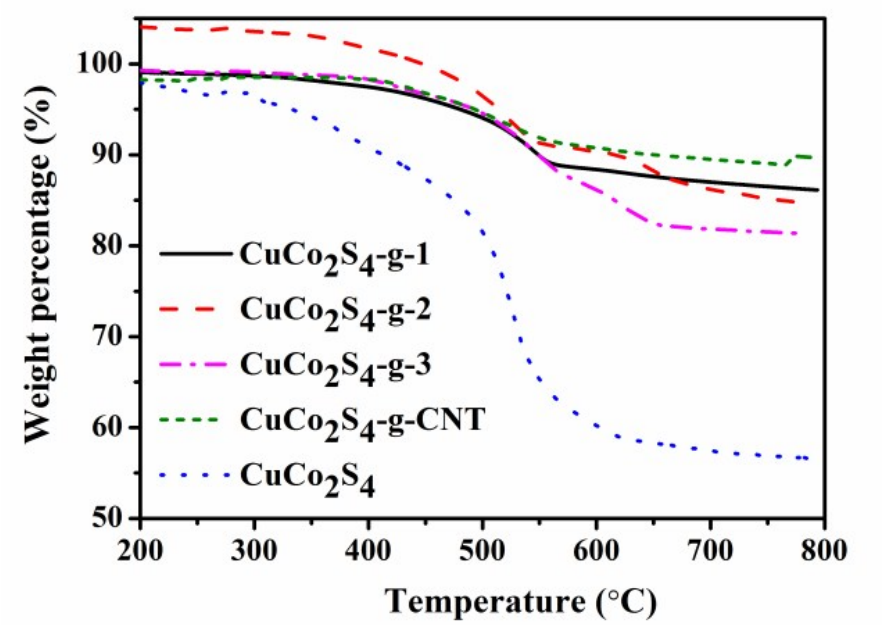

Figure S5 TGA curves of $CuCo_2S_4$, $CuCo_2S_4$-g, and $CuCo_2S_4$-g-CNT.

Figure S5 shows TGA curves of $CuCo_2S_4$, $CuCo_2S_4$-g, and $CuCo_2S_4$-g-CNT. It can be seen that the weight loss of the $CuCo_2S_4$ mainly presents in the range of 400-600 ºC, which is attributed to the thermal decomposition of $CuCo_2S_4$. On the other hand, with the addition of graphene and CNT, the thermodynamic stability of $CuCo_2S_4$ can be greatly improved.

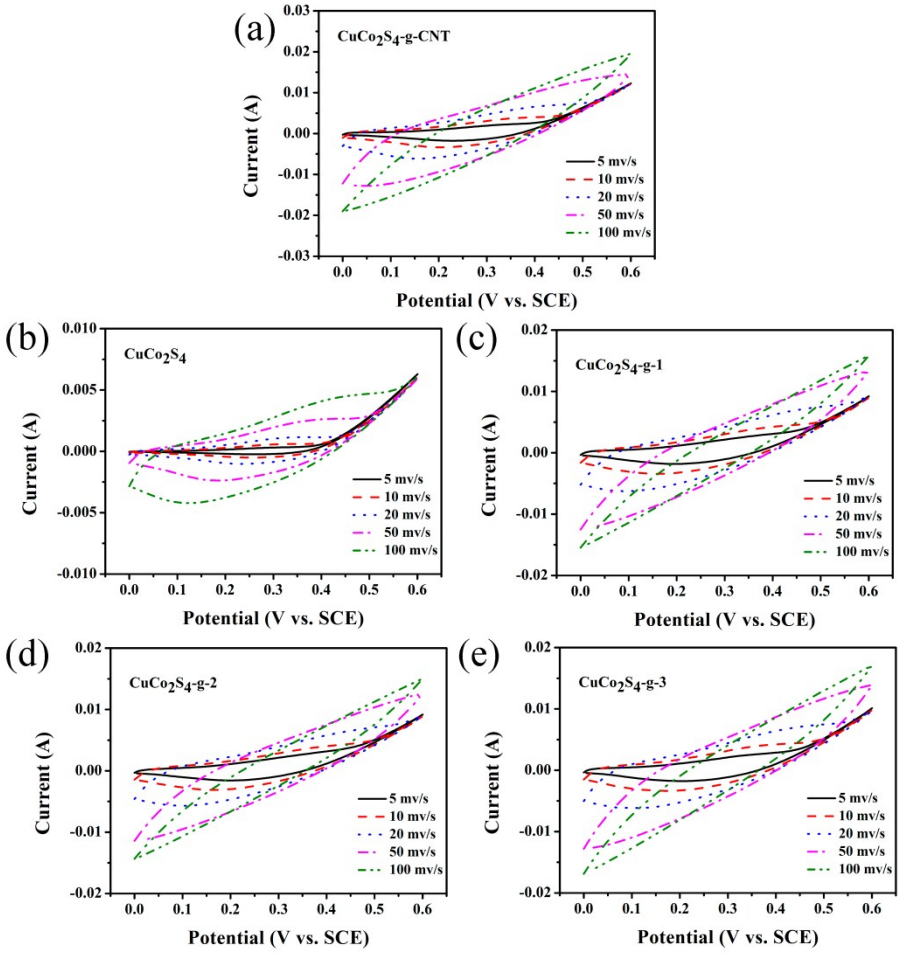

Figure S6 CV curves of $CuCo_2S_4$, $CuCo_2S_4$-g, and $CuCo_2S_4$-g-CNT microstructure at varying scan rates.

Based on the CV measurements, the measured material and device capacitance (C_m, F g^{-1}) can be calculated according to the following equation:

$$C_m = \frac{\int I(V)dv}{vm\Delta V} (F\,g^{-1}) \quad (1)$$

where v is the scan rate (V s^{-1}), m is the mass of the electroactive material in both the positive and negative electrodes (g), and ΔV is the potential window (V).

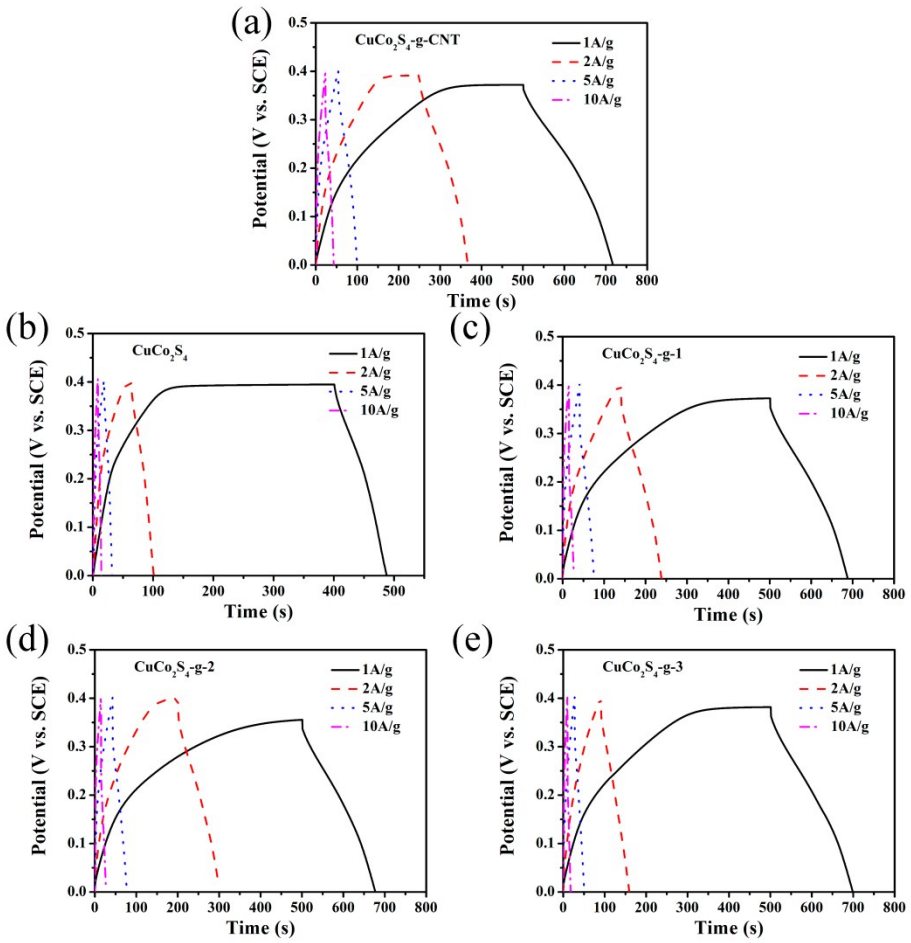

Figure S7 GCD curves of $CuCo_2S_4$, $CuCo_2S_4$-g, and $CuCo_2S_4$-g-CNT at different current densities.

From the GCD curves, the measured capacitance (Cm) can be acquired as follows:

$$C_m = \frac{I\Delta t}{m\Delta V} (Fg^{-1}) \quad (2)$$

where I is the discharge current (A), and Δt is the discharge time (s).

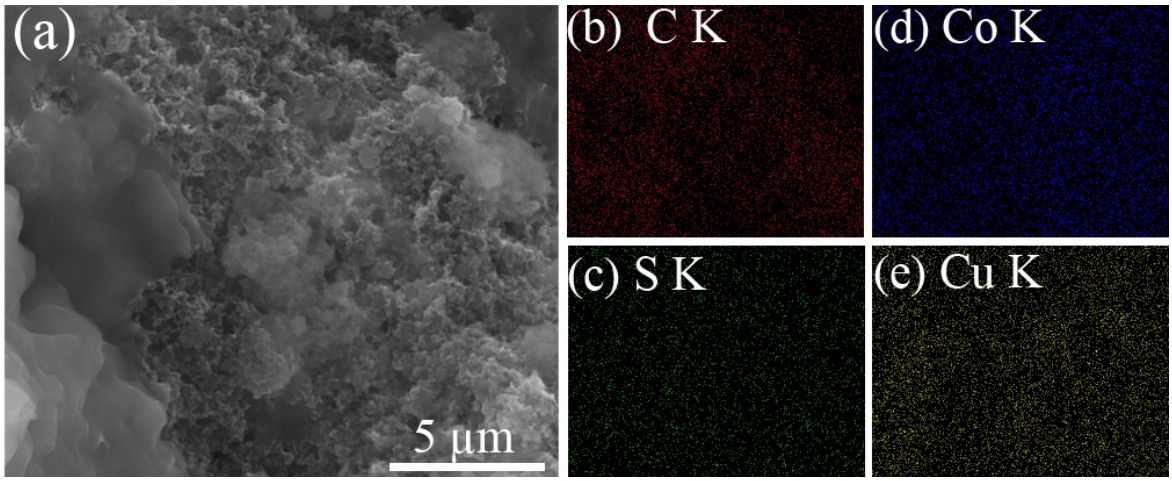

Figure S8 SEM-EDX mapping of $CuCo_2S_4$-g-CNT after cycle test.

From SEM-EDX mapping, it can be found that the structure of $CuCo_2S_4$-g-CNT may slightly change, thus we propose the mechanism for the capacity fading may be the slowly decomposition of active materials.

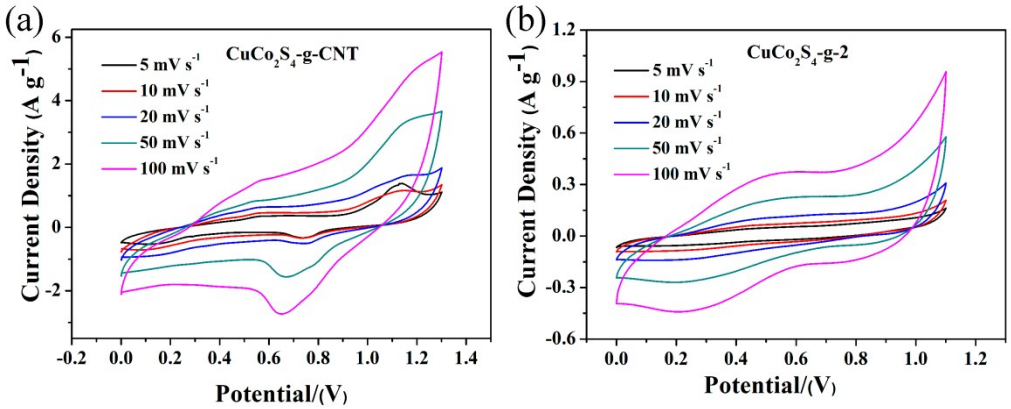

Figure S9 CV curves of $CuCo_2S_4$-g-CNT (a) and $CuCo_2S_4$-g-2 (b) -prepared symmetric devices at different scan rates.

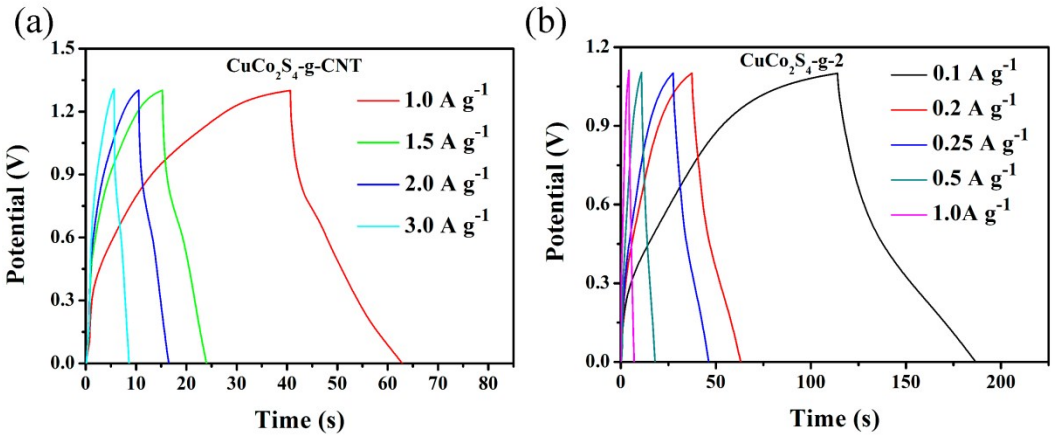

Figure S10 GCD curves of $CuCo_2S_4$-g-CNT (a) and $CuCo_2S_4$-g-2 (b) -prepared symmetric devices at varying current densities.

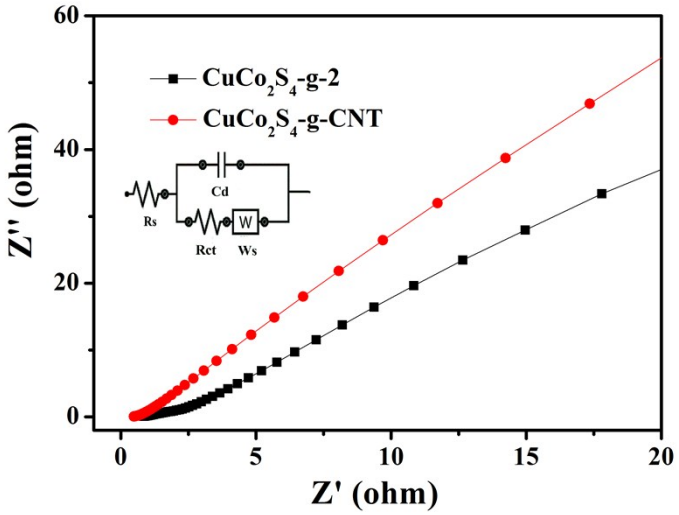

Figure S11 EIS of $CuCo_2S_4$-g-CNT and $CuCo_2S_4$-g-2-prepared symmetric devices.

Figure S11 demonstrates the EIS of $CuCo_2S_4$-g-CNT and $CuCo_2S_4$-g-2-prepared symmetric devices. The depressed circles are attributed to double layer capacitance (Cd), while the interfacial charge transfer resistance (Rct) occurs at the electrode-electrolyte interface. In the low-frequency region, there is a straight line for $CuCo_2S_4$-g-CNT. As well, compared to $CuCo_2S_4$-g-, $CuCo_2S_4$-g-CNT's R_{ct} value is lower. These findings are indicative of excellent capacitive behavior and conductivity.

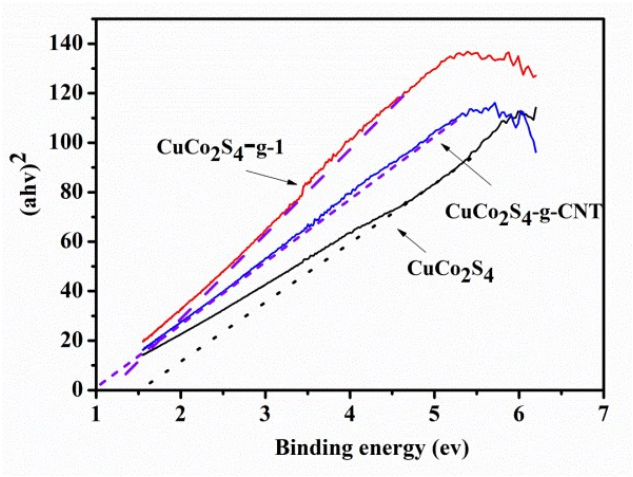

Figure S12 DRS curves of $CuCo_2S_4$, $CuCo_2S_4$-g-1, and $CuCo_2S_4$-g-CNT.

To evaluate the band gaps of $CuCo_2S_4$-containing samples, we characterized the DRS curves of $CuCo_2S_4$, $CuCo_2S_4$-g-2, and $CuCo_2S_4$-g-CNT. Generally, the absorption band gap energy, Eg, is determined according to the following equation:

$$(Ah\nu)^n = K(h\nu - E_g) \quad (3)$$

where hν is the photo-energy, A is the absorbance, K is a constant relative to the material, and n is either 2 for a direct transition, or 1/2 for an indirect transition. For $CuCo_2S_4$, n is 1/2, since it is a semiconductor. From figure S12, note how the addition of CNT greatly decreases the band gap from 2.1 eV ($CuCo_2S_4$) to about 1.2 eV. This trend suggests that the addition of graphene and CNTs improve the conductivity of the samples. In turn, the system is disposed to faster electron transfer.

Table S2 BET specific area of the samples

Sample	BET (m^2/g)
$CuCo_2S_4$	6.163
$CuCo_2S_4$-g-2	12.849
$CuCo_2S_4$-g-CNT	42.981